Particle-in-Cell Modeling of Plasma-Jet Merging in the Large-Hall-Parameter Regime

H. Wen,[1] C. Ren,[2,3] E. C. Hansen,[2] D. Michta,[2] Y. Zhang,[3] S. Langendorf,[4] and P. Tzeferacos[1,2]

[1]Laboratory for Laser Energetics, University of Rochester
[2]Department of Mechanical Engineering, University of Rochester
[3]Department of Physics and Astronomy, University of Rochester
[4]Physics Division, Los Alamos National Laboratory

Plasma-jet–driven magneto-inertial fusion (PJMIF) offers a novel "reactor-friendly" alternative approach to fusion energy that assembles targets by launching magnetized plasma jets from plasma guns at large standoff distances.[1] Fusion reactions take place in an all-gas/plasma architecture, avoiding repetitive hardware destruction. Furthermore, magnetic fields in the assembled target reduce thermal conduction and facilitate ignition. Most of the previous studies on this concept focused on the hydrodynamics,[2–5] while possible kinetic physics,[6] especially in target formation and compression, have not been well explored. Presented here are particle-in-cell (PIC) simulations with the code *OSIRIS* of two colliding counter-propagating magnetized jets to study the kinetic physics in the target formation process. The *OSIRIS* simulation results show that the fuel plasma jets can be stopped due to a microinstability—the modified two-stream instability (MTSI)[7,8]—rather than coulomb collisions. A comparison of 2-D simulations with *OSIRIS* and the single-fluid magnetohydrodynamic code *FLASH* shows that the codes predict similar macroscopic behaviors of the jets stopping and their subsequent expansion, despite the lack of kinetic physics in the *FLASH* simulations. The results provide validation for using *FLASH* to model target formation and beyond for plasma liner experiments (PLX's).

The total ion $v_x - x$ phase space and the spectrum of the longitudinal electric field E_x are shown in Fig. 1 to illustrate the two dominant MTSI modes identified in the simulation. One of the MTSI modes corresponded to the interaction between the incoming ions and the interpenetrated ions from the counter-propagating jet. This MTSI mode is localized in region 1 [locations between the two solid black vertical lines in the ion phase space as shown in Figs. 1(a)–1(c)]. The incoming and interpenetrating jets can be easily identified since the distribution within region 1 has two distinct peaks on the v_x axis. Using the parameters obtained in region 1, we found that the MTSI growth rate was $\gamma_{\mathrm{MTSI}} = 0.1\ \mathrm{ns}^{-1}$ for the fastest growing mode at $k = 0.65\omega_{\mathrm{pe}}/c$, where ω_{pe} is the local plasma frequency and c is the speed of light. The MTSI mode in region 1 initiated a shock that propagated to the left. A localized electrostatic field started to build up across the shock front as the MTSI grew. The interpenetrated ions were accelerated by this field to a longitudinal velocity of about 240 km/s (the sum of the plasma jet velocity and the shock velocity) and sustained that velocity afterward, as illustrated by the phase space features in region 1 in Figs. 1(b) and 1(c). The fastest-growing modes evaluated using parameters obtained from region 1 at different times are overlaid as the black solid line in Fig. 1(d), which agrees reasonably well with the dominant MTSI mode (the bright feature started around $k = 0.7\omega_{\mathrm{pe}}/c$ at $t \approx 70$ ns), including the shift to lower k at a later time. The other MTSI mode (first appeared around $t \approx 85$ ns with $k = 1.2\omega_{\mathrm{pe}}/c$) in Fig. 1(d) corresponded to the interaction between the incoming ions and the reflected ions. This MTSI mode was localized in region 2, locations between the two dashed vertical lines in Figs. 1(b) and 1(c), which tracked the shock-front propagation. Figure 1(d) plots the fastest-growing MTSI mode as a dashed black line that agreed well with the bright feature to the right of the initial MTSI mode corresponding to region 1. As evident in Fig. 1(d), this MTSI mode occurred later than the initial MTSI mode because the shock was generated by the initial MTSI mode. The wave number k_x of these two MTSI modes both shifted to smaller values over time, mainly due to the decreasing density and magnetic field in regions 1 and 2.

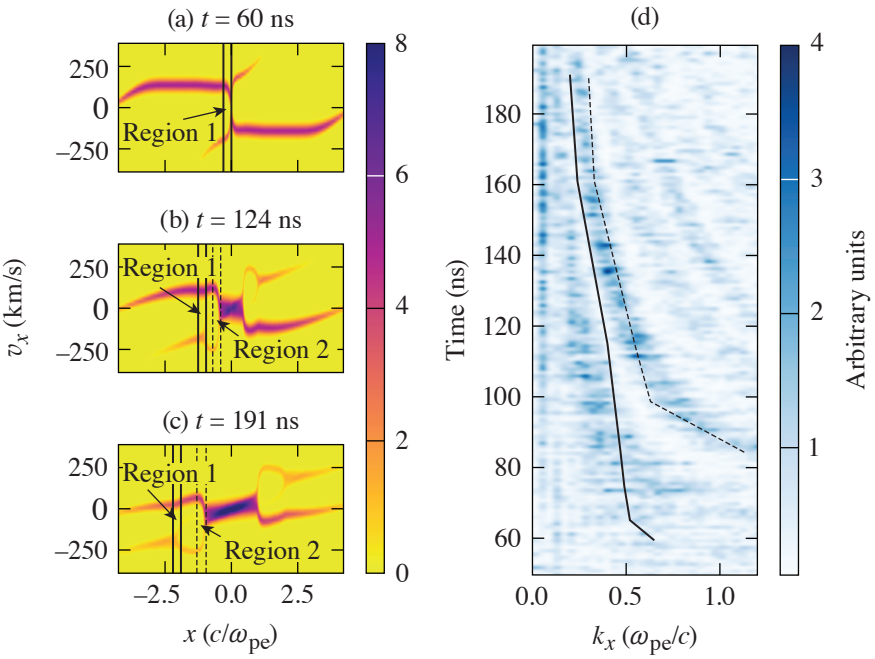

TC16003JR

Figure 1
Ion v_x–x phase space at (a) $t = 60$ ns, (b) $t = 124$ ns, and (c) $t = 191$ ns; (d) the spectrum of longitudinal electric field E_x. The solid and dashed black lines in the plot (d) correspond to the fastest-growing MTSI modes with parameters obtained from the regions 1 and 2 [plots (a)–(c)], respectively.

Figure 2 shows the time evolution of the plasma β, the electron Hall parameter χ_e, and the ion Hall parameter χ_i in the central merging region obtained from *OSIRIS* and *FLASH* simulations. The dimensionless parameters predicted by the two codes were on the same order of magnitude. During the jet-merging process and before the merged plasma expansion, i.e., between 50 and 200 ns, χ_e, and χ_i were greater than unity; the plasma β was close to unity. This is the desired characteristic of planned PLX. The same level of agreement between the two codes was achieved for the electron and ion Hall parameters. The plasma β differed more in the antiparallel-B case: β in *OSIRIS* was consistently larger than in *FLASH*. This is likely due to the interpenetrated species carrying magnetic fields to the other jet, leading to the enhanced magnetic-field cancellation.

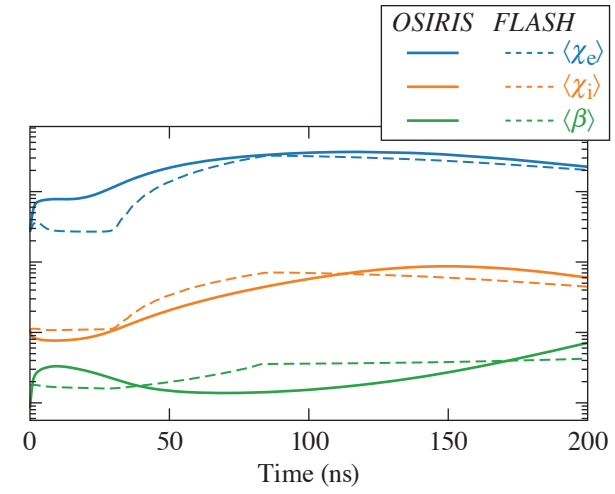

TC16011JR

Figure 2
The dimensionless parameters near the merging region obtained in *OSIRIS* (solid lines) and *FLASH* (dashed lines) simulations of a 5-eV plasma jet collision: electron Hall parameter $\langle\chi_e\rangle$ parameter (blue lines), ion Hall parameter $\langle\chi_i\rangle$ (orange lines), and plasma $\langle\beta\rangle$ (green lines). The angle bracket corresponds to spatial average.

In summary, the MTSI is identified to be the main mechanism responsible for stopping the plasma jets and preventing species interpenetration. The 2-D PIC simulations validate the results of the radiation magneto-hydrodynamics code *FLASH*, which will be the primary tool for modeling various stages of future PJMIF experiments.

This material was based upon the work supported, in part, by the Advanced Research Projects Agency-Energy (ARPA-E), U.S. Department of Energy (DOE), under Award Nos. DE-AR0001272and DE-SC0020431; by the U.S. DOE National Nuclear Security Administration (NNSA) under Award No. DE-NA0003856; the University of Rochester; and the New York State Energy Research and Development Authority. This manuscript has been authored in collaboration with Los Alamos National Laboratory/Triad National Security, LLC, Contract No. 89233218CNA000001, with the U.S. Department of Energy/National Nuclear Security Administration. This research used resources of the National Energy Research Scientific Computing Center (NERSC), a U.S. Department of Energy Office of Science User Facility located at the Lawrence Berkeley National Laboratory, operated under Contract No. DE-AC02-05CH11231 using NERSC Award No. FES-ERCAP0017949.

1. S. C. Hsu and S. J. Langendorf, J. Fusion Energy **38**, 182 (2019).
2. J. S. Davis *et al.*, Phys. Plasmas **19**, 102701 (2012).
3. J. T. Cassibry, M. Stanic, and S. C. Hsu, Phys. Plasmas **20**, 032706 (2013).
4. W. Shih *et al.*, Phys. Plasmas **26**, 032704 (2019).
5. K. Schillo and J. Cassibry, Phys. Plasmas **27**, 042707 (2020).
6. C. Thoma, D. R. Welch, and S. C. Hsu, Phys. Plasmas **20**, 082128 (2013).
7. J. B. McBride *et al.*, Phys. Fluids **15**, 2367 (1972).
8. S. P. Gary, *Theory of Space Plasma Microinstabilities*, Cambridge Atmospheric and Space Science Series (Cambridge University Press, Cambridge, 1993).